KECK Geology Consortium
Learning Science Through Research
Published by Keck Geology Consortium
Short Contributions
29th Annual Symposium Volume
23rd April, 2016
ISBN: 1528-7491

ANTARCTIC WEDDELL SEA ODP SITE 697 SEDIMENTOLOGICAL CHANGES

KATE CULLEN, Wesleyan University
Research Advisor: Professor Suzanne OConnell

INTRODUCTION

Pliocene Antarctic Glacial History

As climate change intensifies and people begin to feel its impacts, scientists are looking to past climatically similar periods to understand how our planet will respond. The Pliocene Epoch (5.33-2.58 million years ago) is the last interval in which global CO_2 concentrations were the same as at present—400 parts per million (Fedorov et al., 2013). During the Pliocene Climatic Optimum (see Table 1, OConnell) the West Antarctic Ice Sheet (WAIS) nearly de-glaciated under peak CO_2 concentrations and global average temperatures 2-3°C warmer than pre-industrial values (Yamane et al., 2015). These climatic conditions were likely driven by an obliquity orbital forcing, which increases insolation at polar latitudes (Naish et al., 2009). Climate models suggest that the WAIS was sensitive to atmosphere and ocean temperature fluctuations (DeConto and Pollard, 2003). A larger question is how sensitive the East Antarctic Ice Sheet (EAIS) was to the same forcing. Recent data from Wilkes Land (Cook et al., 2007), suggest that large segments of the EAIS melted during the Pliocene. This study utilizes XRF counts and spectral analysis of marine sediment cores from Weddell Sea ODP Site 697 to identify sedimentological changes that can be linked to ice sheet dynamics.

The International Ocean Discovery Program

The International Ocean Discovery Program (IODP), formerly known as the Ocean Drilling Program (ODP), is a scientific deep-sea drilling collaboration that collects ocean floor geological data for research on Earth dynamics and history. Sediment cores for this study were recovered in January and February of 1987 on ODP Expedition 113 to the Weddell Sea, Antarctica. Cores from Hole 697B (61°48.626'S, 40°17.749'W) in the Jane Basin north of the Antarctic Peninsula (OConnell, Fig. 1) were selected for analysis because they contain sediment from both the WAIS and EAIS, have relatively high sedimentation rates and a paleomagnetic reversal stratigraphy for age control.

METHODS

X-Ray Fluorescence

X-Ray Fluorescence (XRF) spectroscopy is an analytical technique used as a means of determining major and trace element concentrations of a particular material. Cores were scanned by a third-generation AVAATECH® XRF Core Scanner at the IODP Texas headquarters at Texas A&M in College Station, Texas. Surficial scans were taken down the center of the core at 2 cm intervals, skipping uneven or cracked areas, with an X-ray illumination area of 1 cm^2. All core sections were scanned at 10 kV and 30 kV to detect major elements and heavy trace elements. The cores were then imaged with the Ocean Drilling Program Core Imaging Machine, providing a .tif file and high-resolution RGB data excel file for each core section and scanned for magnetic susceptibility.

To account for water loss, each core section was stretched to its initial shipboard recorded length and the XRF elemental accounts were interpolated across the new range. The depth measurements within each individual core were converted to a meters below sea

floor measurements by adding the distance of the core top to the sea floor to the depth measurement within the core. Meter below sea floor core measurements were transformed from a depth scale to age by interpolating the ages of all depths between the known ages of magnetic reversals. The magnetic time scale of Gee & Kent, 2007 was used to date the magnetic reversal pattern from Hamilton & O'Brien, 1990 (in Pudsey, 1990).

Magnetic Susceptibility

Magnetic susceptibility provides a dimensionless value that reflects the total amount of magnetic material present in a given interval of sediment. Site 697 cores were run through a multi-track sensor at the IODP Texas headquarters to collect magnetic susceptibility values. Measurements were taken at 0.1 cm intervals down the center of the core and recorded in an .ms (magnetic susceptibility) file. The .ms files were converted to .csv file in R Studio and interpolated. Meters below sea floor and age values were then calculated. Unusually high measurements that correspond to a drop stone were removed.

Spectral Reflectance

Spectral reflectance analysis was used to identify the mineral composition of thirty-six sediment samples. This procedure identifies the presence of common minerals in the sediment sample, but not abundance. Core samples were taken at the IODP Texas headquarters and sorted into coarse (>500 μm), (150-500 μm) and fine sand fractions (63-150 μm) at Wesleyan. Fine-fraction samples (silt and clay < 63 μm) from Cores 13X through 17X, approximately 3.03 Ma through 3.77 Ma, were identified for spectral analysis and mineral identification. Samples chosen contain high or low coarse fraction (>63 μm) weight percent and/or high or low biosilica weight percent.

Reflectance spectra were obtained using an ASD Fieldspec FR® spectro-radiometer with a wavelength range of 350–2500nm. Readings were taken at an interval of 1.4nm between 350–1000nm and 2nm between 1000–2500nm at a spectral resolution of 3nm between 350–1000nm and 10nm between 1000–2500nm. Spectra were taken by hand-positioning a 25° field of view fiber optic sensor 10 cm above the fine fraction sediment sample under uniformed, artificial light. The <63 um fraction settled in a 1 liter plastic bucket. Water was decanted and when < 3 cm of liquid remained, the samples were air dried. Silt grains settled first and as a result most samples had two distinct sides, a light silt fraction on the bottom toped with a dark, shinny clay fraction. Spectra were taken on each sides of the sample. Ten measurements were taken per scan, converted to ASCII files using SpecPro and averaged in Excel to provide a single spectrum for each target. Spectra were normalized to a white Spectralon® panel.

RESULTS

Elemental Count Ratios

Iron (Fe) to titanium (Ti) ratio and silica (Si) to titanium (Ti) ratios were created using XRF count data. Elemental count ratios were normalized with titanium to account for terrigenous sources of sediment deposition. Titanium reaches the Jane Basin predominantly from land and does not affect biogeochemical cycles. Both ratios are helpful comparisons to paleoproductivity indicators such as average biosilica weight percent.

Clay Mineral Identification

Reflectance spectra were inputted to XQuartz 2.7.7 ENVI 5.1 and ENVI Classic for mineral identification. The collected spectra were then individually compared to the USGS mineral spectra library. Minerals displaying similar spectral behavior were preliminarily identified. To verify the match, the major pronouncements (mineral-specific absorption points) of each collected spectra and each relevant library spectra were recorded and compared.

Smectite, in the form of montmorillonite, is the most consistently identified mineral. This finding is consistent with a study performed in Robert & Maillot, 1990 on the same core sections. Montmorillonite has a large presence in Cores 13X, 15X, 16X and 17X, but a limited presence in Core 14X. Robert & Maillot, 1990 found smectite to form more than 40% of all clay minerals throughout these samples, with highest smectite abundance in Cores 13X and 16X and lowest abundance in Core 14X.

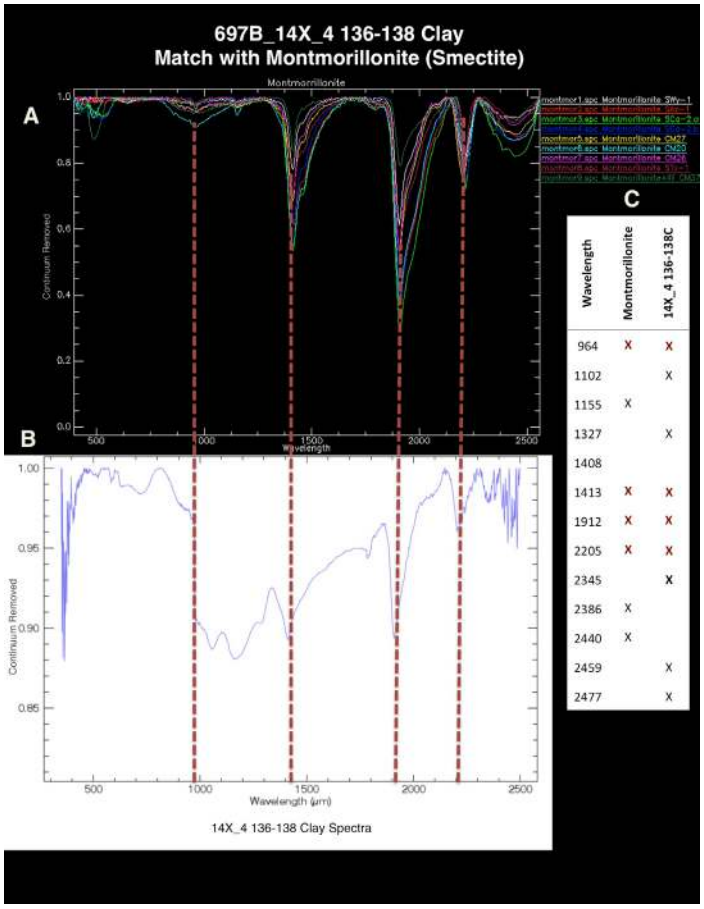

Figure 1. Mineral Identification Procedure.
A and B. The montmorillonite (smectite) spectra from the USGS library in comparison to the clay Sample 14X_4 136-138. Both spectra are plotted as a continuum removed data spectrum against wavelength in micrometers.
C. This table shows the verification procedure for matching spectra behavior from a collected sample to the mineral-specific pronouncements at wavelength values.

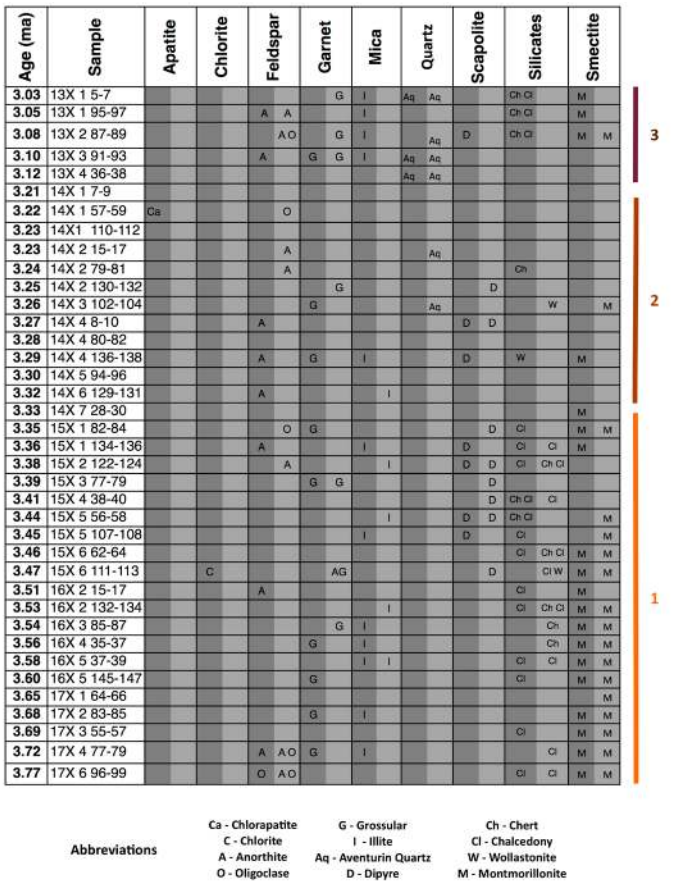

Age (ma)	Sample	Apatite	Chlorite	Feldspar	Garnet	Mica	Quartz	Scapolite	Silicates	Smectite	
3.03	13X 1 5-7				G	I	Aq Aq		Ch Cl	M	
3.05	13X 1 95-97			A A		I			Ch Cl	M	
3.08	13X 2 87-89			A O	G	I	Aq	D	Ch Cl	M	M
3.10	13X 3 91-93			A	G G	I	Aq Aq				
3.12	13X 4 36-38						Aq Aq				
3.21	14X 1 7-9										
3.22	14X 1 57-59	Ca		O							
3.23	14X1 110-112										
3.23	14X 2 15-17			A			Aq				
3.24	14X 2 79-81			A					Ch		
3.25	14X 2 130-132				G			D			
3.26	14X 3 102-104				G		Aq		W		M
3.27	14X 4 8-10			A				D D			
3.28	14X 4 80-82										
3.29	14X 4 136-138			A	G	I		D	W	M	
3.30	14X 5 94-96										
3.32	14X 6 129-131			A		I					
3.33	14X 7 28-30									M	
3.35	15X 1 82-84			O	G			D	Cl	M	M
3.36	15X 1 134-136			A		I		D	Cl Cl	M	
3.38	15X 2 122-124			A		I		D D	Cl Ch Cl		
3.39	15X 3 77-79				G G			D			
3.41	15X 4 38-40							D	Ch Cl Cl		
3.44	15X 5 56-58					I		D D	Ch Cl		M
3.45	15X 5 107-108					I		D	Cl		M
3.46	15X 6 62-64								Cl Ch Cl	M	M
3.47	15X 6 111-113		C		AG			D	Cl W	M	M
3.51	16X 2 15-17			A					Cl	M	
3.53	16X 2 132-134					I			Cl Ch Cl	M	M
3.54	16X 3 85-87				G	I			Ch	M	M
3.56	16X 4 35-37				G	I			Ch	M	M
3.58	16X 5 37-39					I I			Cl Cl	M	M
3.60	16X 5 145-147				G				Cl	M	M
3.65	17X 1 64-66										M
3.68	17X 2 83-85				G	I				M	M
3.69	17X 3 55-57								Cl	M	M
3.72	17X 4 77-79			A	A O G	I				Cl	M M
3.77	17X 6 96-99			O	A O				Cl	Cl	M M

3
2
1

Abbreviations

Ca - Chlorapatite
C - Chlorite
A - Anorthite
O - Oligoclase

G - Grossular
I - Illite
Aq - Aventurin Quartz
D - Dipyre

Ch - Chert
Cl - Chalcedony
W - Wollastonite
M - Montmorillonite

Figure 2. 697B 13X-17X Fine Fraction Mineral Identification. The presence of a mineral in a particular sample is indicated with the initial of its mineral name under its mineral category. Each category is split into a clay (dark grey) and silt (light grey) section to clarify whether the mineral was identified on the clay or silt side of the fine sediment sample. Section 1 samples are characterized by high smectite, silicate, quartz, mica, garnet, and feldspar presence. Section 2 samples show high smectite, silicate and scapolite presence, and moderate illite, garnet and feldspar presence. Section 3 samples show very high smectite and silicate presence, and moderate to high illite and garnet presence.

In contrast to Robert & Maillot, 1990, neither amphiboles nor kaolinite were found. Chlorite was identified only once. A possible explanation for this discrepancy is that the 1990 studies analyzed a < 2 µm fraction using a standard clay mineral preparation and samples were measured with a Philips Diffractometer. This study analyzed the <63 µm sample with a spectro-radiometer.

The carbonate minerals calcite and dolomite were not found. The silicate minerals chert and chalcedony are found consistently throughout the samples, except in Core 14X. Chalcedony, a cryptocrystalline silicate rock with fine intergrowths of quartz and moganite, was present in the top of Core 13X (deposited 3.03-3.07 Ma) as well as between Cores 15X and 17X (3.34-3.77 Ma). Chert, which is another silicate rock that can form from biosilica diagenesis, was also identified in many of these samples. Wollastonite, a calcium silicate mineral, was identified in Core 14X.

Apatite and chlorite minerals are found only once. Feldspar is distributed evenly throughout Cores 13X and 14X, but mostly absent between the base of 14X and the base of Core 17X. Garnet and mica are distributed evenly throughout all cores. Aventurin quartz is one of the few quartz minerals identifiable with the ASD Fieldspec FR® spectro-radiometer. It has a high presence in Core 13X and limited presence in Core 14X. Other forms of quartz could also be

A

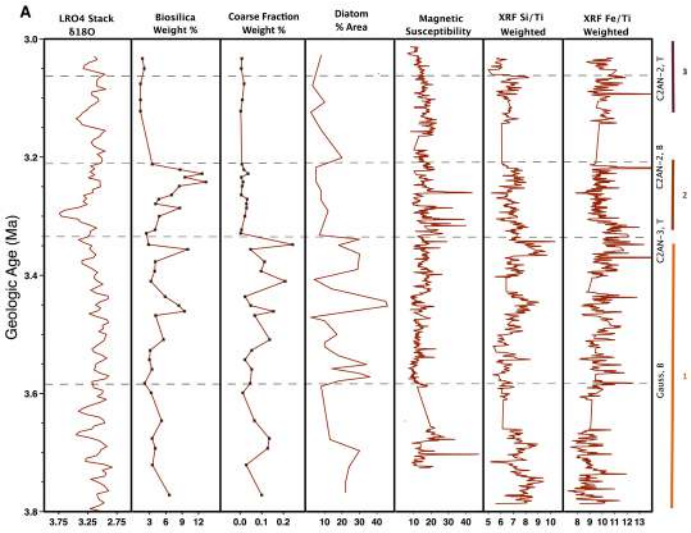

B

	Mineral Presence	2016 Biosilica and IRD	1990 Diatoms	Magnetic Susceptibility	Si/Ti and Fe/Ti
Section 3 ~3-3.1 Ma	High M, Cl, Ch, Aq, I, G, A	Low biosilica and IRD wt. %	Low diatom % area	Moderate, non-volatile behavior	More erratic Fe/Ti than Si/Ti behavior
Section 2 ~3.2-3.3 Ma	Mod M, W, D, Aq, G, A	Variable and increasing biosilica, low and consistent IRD behavior	Low, consistent diatom behavior	Higher peaks and steep decreases	More volatile behavior, higher Fe/Ti than Si/Ti values
Section 1 ~3.3-3.7 Ma	High M, Cl, Ch, D, I, G, A	Variable IRD and biosilica, biosilica peaks lead or occur simultaneously with IRD 3.54 Ma and later lower biosilica and IRD	Peaks and valleys align inversely with IRD and biosilica peaks and valleys	Moderate behavior and low values	Peaks seem to align with or lead diatom peaks

Figure 3. 13X-17X Elemental Counts Comparison to Paleoclimate Proxies
A. Section 1, 2 and 3 from Figure 3 are illustrated for comparison to mineral deposition behavior. The LRO4 stack is included as a proxy of global temperature and glacial behavior (Lisiecki & Raymo, 2005). Biosilica weight percent was performed at Wesleyan in 2015-2016 [See C. Flores Keck Paper 2016] and diatom percent area is from Pudsey, 1990. They are included as paleoproductivity indicators. Coarse fraction weight percent is included as an indicator of ice rafted debris (IRD) behavior. Magnetic susceptibility is included for comparison to IRD. XRF Si/Ti and Fe/Ti five-point weighted averages are included for comparison to biosilica and diatom data.
B. This table summarizes behavior of all climate indicators for each identified section.

A.

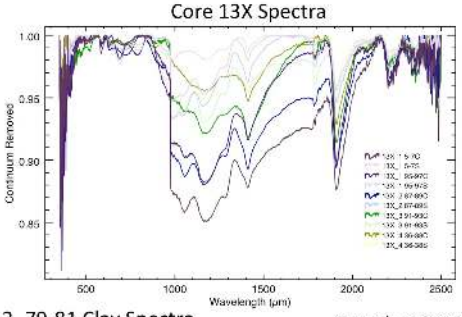

B.

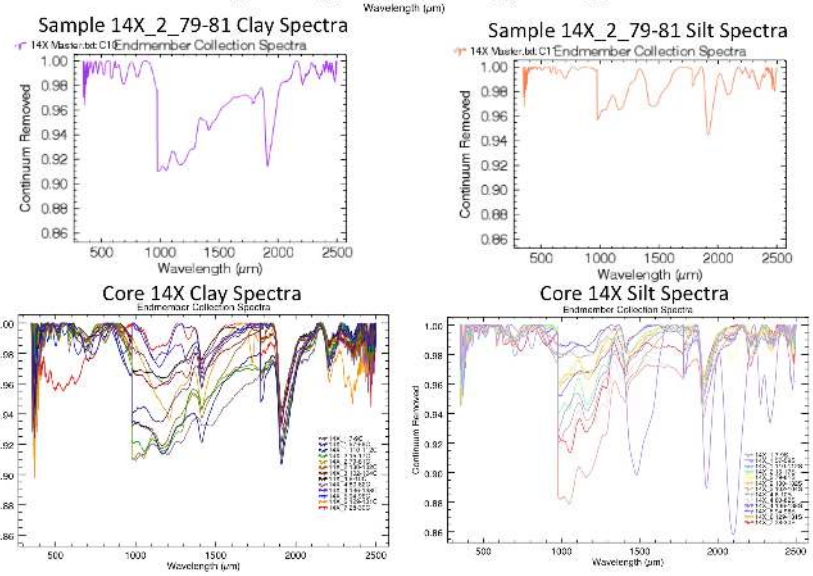

Figure 4. Clay and Silt Spectra for Core 13X and Core 14X
A. Clay and silt spectra are displayed together for Core 13X samples. Silt spectra are in lighter colors and clay spectra are in darker colors. The silts have visibly higher spectra than the clays. This visible difference between clay and silt spectra was present in most spectra collected.
B. Clay and Silt spectra for Core 14X
The clay and silt spectras for Core 14X, Section 2, Sample79-81 is displayed. This sample was chosen because biosilica weight percent highest of all samples collected for this study at 13.35%. Coarse fraction weight percent moderate at 1.3% and diatom content moderate at 14 percent of smear slide area. Magnetic susceptibility, Fe/Ti and Si/Ti ratios also moderate compared to other values. The spectras for all clays and all silt samples in Core 14X are displayed below for comparison.

present, but were not detected. Dipyre, which is a scapolite that forms in the presence of small amounts of chlorine, was identified in Cores 14X and 15X.

Chert, chalcedony, illite, grossular and anorthite are often identified on either the clay or silt side of a sediment sample and not both. Montmorillonite is more often identified on both sides of a sample.

As indicated in Figure 2, samples in Cores 13X-17X can be grouped into three sections that describe different clay mineral compositions. Section 1 spans from ~3.3-3.7 Ma (149.25-175.67 mbsf) and is characterized by high smectite and silicate deposition and consistent illite and garnet deposition. Section 2 (~3.2-3.3 Ma, 138.78-147 mbsf) contains consistent smectite, silicate, scapolite, quartz, illite, garnet and feldspar deposition. Section 3 (~3-3.1 Ma, 138.78-133.47 mbsf) is characterized by presence of smectite, silicate, quartz, illite, garnet, and feldspar.

DISCUSSION AND CONCLUSION

Clay minerals carry useful information about sediment transport and depositional mechanisms as well as climate changes in the sediment source area on adjacent landmasses (Fagel, 2007). This study shows that clay mineral deposition behavior may have a relationship with climate proxy indicators for Site 697B in the Jane Basin, Weddell Sea. The three sections of mineral deposition identified in this study also correspond to three different patterns of behavior in elemental count ratios, biosilica, diatom, and IRD data (Figure 3).

More information on the climate forcing for sediment deposition is helpful because paleoclimate proxies are not always compatible. For example, the relationship between diatom percent of area data and sand percent (indicative of IRD) is not statistically significant (Figure 4, Pudsey, 1990). The relationship between the coarse fraction weight percent and biosilica weight percent is also not statistically significant (Figure 4).

ACKNOWLEDGEMENTS

I would like to thank Professor Suzanne O'Connell for her tireless support and mentorship. I would also like to thank Professor Martha Gilmore for her guidance with spectral reflectance analysis. A special thanks to Eduardo Centeno for his assistance with spectra collection and of course to Cindy Flores, Zack Kaufman, Elena Robakiewicz and the growing Team Antarctica family. Thank you to the Keck Geology Consortium, National Science Foundation, ExxonMobil Corporation and Wesleyan's College of the Environment for supporting this project. And

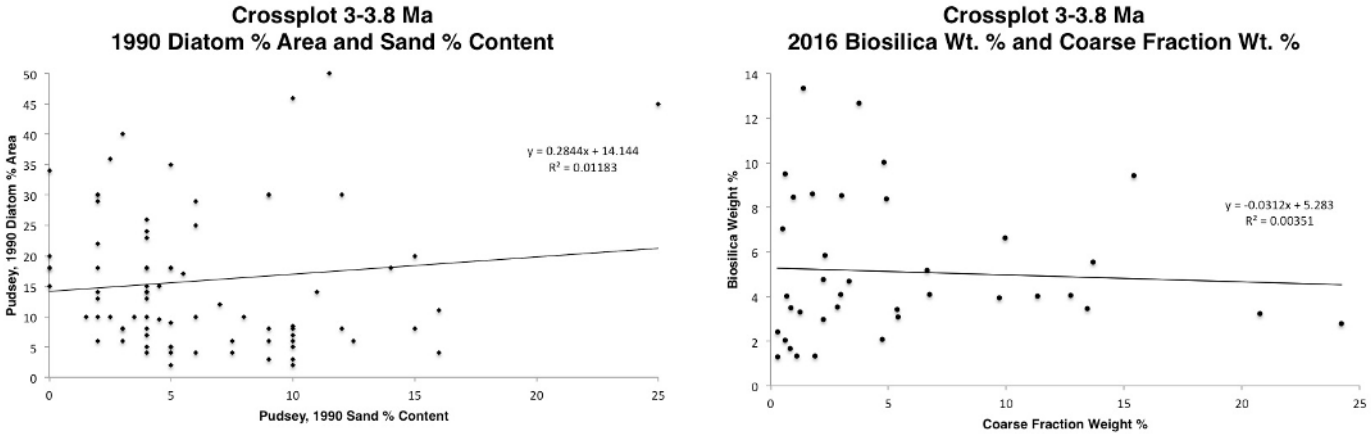

Figure 5. Crossplots of Biosilica v. Ice Rafted Debri (IRD) for 1990 and 2016
Data for A. and B. includes only includes points from Cores 13X-17X where mineral identification was performed.
A. Crossplot of Pudsey, 1990 sand percent content (indicative of IRD content) compared to diatom percent area of a smear slide.
B. Crossplot of Wesleyan University Professor O'Connell lab weight percent of coarse fraction (from Kaufman, 2016, indicative of IRD content) compared to biosilica weight percent from 2016.

finally, thank you to the International Ocean Discovery Program for providing sediment cores and Claire McKinley for assistance at the Texas A&M IODP Repository.

REFERENCES

Barker, P.E, Kennett, J.P., et al., 1988. *Proc. ODP, Init. Repts.,* 113: College Station, TX (Ocean Drilling Program).

Deconto, R.M., and Pollard, D. (2003). Eapid Cenozoic glaciation of Antarctica induced by declining atmospheric CO2. *Nature, 421*(6920), 245-249.

Fagel, N. (2007). Clay Minerals, Deep Circulation and Climate. *Development in Marine Geology,* Vol. 1, pp. 139-184.

Fedorov, A.V., Brierley, C. M., Lawrence, K. T., Liu, Z., Dekens, P.S., Ravelo, A.C. (2013) Patterns and Mechanisms of early Pliocene warmth. Nature, Vol. 496, pp. 43–49. doi:10.1038/nature12003.

Gee, J. S., & Kent, D. V. (2007). Source of oceanic magnetic anomalies and the geomagnetic polarity time scale. *Treatise on Geophysics, Vol. 5: Geomagnetism*, 455-507.

Lisiecki, L. E., & Raymo, M. E. (2005). A Pliocene-Pleistocene stack of 57 globally distributed benthic δ18O records. *Paleoceanography*, *20*(1).

Naish, T., Powell, R., Levy, R., Wilson, G., Scherer, R., Talarico, F., Krissek, L., Niessen, F., Pompilio, M., Wilson, T. and Carter, L., 2009. Obliquity-paced Pliocene West Antarctic ice sheet oscillations. *Nature, 458* (7236), pp. 322-328.

Raymo, M.E., Pearty, P., De Conto, R., O'Leary, M., Dowsett, H.J., Robinson., M.M., Mitrovica, J.X. (2009) PLIOMAX: Pliocene maximum sea level project, PAGES News Vol. 17, pp.58-59.

Robert, C., and Maillot, H., 1990. Paleoenvironments in the Weddell Sea area and Antarctic climates, as deduced from clay mineral associations and geochemical data, ODP Leg 113.*In* Barker, P.F., Kennett, J.P., et al., *Proc. ODP, Sci. Results,* 113: College Station, TX (Ocean Drilling Program), 51–70.

Shipboard Scientific Party, Site 697. (1988) Barker P.F., Kennett, J.P. Proc. ODP, Initial Reports, 113, College Station, TX (Ocean Drilling Program), p. 705-774.

Pagani, M., Liu, Z., LaRiviere, J., & Ravelo, A. C. (2010). High Earth-system climate sensitivity determined from Pliocene carbon dioxide concentrations. Nature Geoscience, 3(1), 27-30.

Pudsey, C.J., 1990. Grain size and diatom content of hemipelagic sediments at Site 697, ODP Leg 113: a record of Pliocene–Pleistocene climate. In Barker, P.F., Kennett, J.P., et al., *Proc. ODP, Sci. Results,* 113: College Station, TX (Ocean Drilling Program), 111–120.

Yamane, Masako, Yusuke Yokoyama, Ayako Abe-Ouchi, Stephen Obrochta, Fuyuki Saito, Kiichi Moriwaki, and Hiroyuki Matsuzaki. "Exposure Age and Ice-Sheet Model Constraints on Pliocene East Antarctic Ice Sheet Dynamics." Nature Communications, 6, 7016.